Fibronectin fibril alignment is established upon initiation of extracellular matrix assembly

Carly M. Garrison and Jean E. Schwarzbauer*
Department of Molecular Biology, Princeton University, Princeton, NJ 08544

ABSTRACT **The physical structure of the extracellular matrix (ECM) is tissue-specific and fundamental to normal tissue function. Proper alignment of ECM fibers is essential for the functioning of a variety of tissues. While matrix assembly in general has been intensively investigated, little is known about the mechanisms required for formation of aligned ECM fibrils. We investigated the initiation of fibronectin (FN) matrix assembly using fibroblasts that assemble parallel ECM fibrils and found that matrix assembly sites, where FN fibrillogenesis is initiated, were oriented in parallel at the cell poles. We show that these polarized matrix assembly sites progress into fibrillar adhesions and ultimately into aligned FN fibrils. Cells that assemble an unaligned meshwork matrix form matrix assembly sites around the cell periphery, but the distribution of matrix assembly sites in these cells could be modulated through micropatterning or mechanical stretch. While an elongated cell shape corresponds with a polarized matrix assembly site distribution, these two features are not absolutely linked, since we discovered that transforming growth factor beta (TGF-β1) enhances matrix assembly site polarity and assembly of aligned fibrils independent of cell elongation. We conclude that the ultimate orientation of FN fibrils is determined by the alignment and distribution of matrix assembly sites that form during the initial stages of cell–FN interactions.**

Monitoring Editor
Valerie Marie Weaver
University of California, San Francisco

Received: Aug 14, 2020
Revised: Jan 19, 2021
Accepted: Feb 18, 2021

INTRODUCTION

The three-dimensional organization of extracellular matrix (ECM) is complex; appropriate assembly of features ranging from nanometer to micrometer scale is needed to provide spatial and mechanical cues that regulate cell behavior such as migration, differentiation, and proliferation (Frantz *et al.*, 2010). Each tissue has a unique ECM composition and architecture that are essential for its particular function (Kjaer, 2004; Frantz *et al.*, 2010; Burgstaller *et al.*, 2017; Eyckmans and Chen, 2017; McKee *et al.*, 2019). ECM in the tissue stroma, such as in the breast, salivary gland, skin, and prostate, is usually composed of a meshwork of ECM fibrils without a predominant global fibril orientation (Bosman and Stamenkovic, 2003; Paszek and Weaver, 2004). However, certain tissues exhibit aligned ECM organization, with fibrils oriented in linear arrays, parallel to one another. Proper alignment of ECM fibers is essential for the function of tissues such as the corneal stroma, bones, tendons, skeletal muscle, and vasculature (Canty *et al.*, 2006; Lanfer *et al.*, 2008; Hassell and Birk, 2010; Li *et al.*, 2014; Meek and Knupp, 2015). The critical importance of aligned matrices in these tissues is made clear by the impairment of normal function when this distinct organization is lost. For example, after tendon injury, healing is usually insufficient to restore collagen fiber alignment and native tissue architecture (Galloway *et al.*, 2013). In contrast, formation of aligned ECM in environments where there is normally unoriented matrix is often detrimental to health. Specifically, the presence of aligned ECM fibrils around solid tumors is correlated with poor patient prognosis and is thought to facilitate outmigration of tumor cells and promote local invasion into surrounding tissue (Provenzano *et al.*, 2006, 2008; Conklin *et al.*, 2011; Hanley *et al.*, 2016; Erdogan *et al.*, 2017). While matrix assembly in general has been intensively investigated and basic principles have been

This article was published online ahead of print in MBoC in Press (http://www.molbiolcell.org/cgi/doi/10.1091/mbc.E20-08-0533) on February 24, 2021.

Author contributions: C.M.G. and J.E.S. conceived and designed experiments; C.M.G. performed the experiments; C.M.G. and J.E.S. analyzed the data; C.M.G. and J.E.S. drafted the article; C.M.G. prepared the digital images.

Conflicts of interest: The authors declare no conflicts of interest.

*Address correspondence to: Jean Schwarzbauer (jschwarz@princeton.edu).

Abbreviations used: BSA, bovine serum albumin; ECM, extracellular matrix; FN, fibronectin; MAS, matrix assembly site; TGF-β1, transforming growth factor beta 1; TIRF, total internal reflection fluorescence.

elucidated, the mechanisms required for de novo assembly of aligned ECM fibers are not well understood.

Although the composition and structure of the ECM is unique from tissue to tissue, most matrices contain the ubiquitous ECM protein fibronectin (FN; Frantz *et al.*, 2010; Singh *et al.*, 2010). FN is considered to be a "foundational matrix" because other ECM components depend upon the presence of FN for their incorporation into the ECM. For example, the assembly of FN into a stable matrix is necessary for fibrillogenesis of several types of collagen (Sottile and Hocking, 2002; Velling *et al.*, 2002; Sottile *et al.*, 2007; Miller *et al.*, 2014) and of fibrillin-1 (Kinsey *et al.*, 2008; Sabatier *et al.*, 2009). Thus, ECM alignment may initially be organized through the formation of aligned FN fibrils that then act as a template for assembly of other ECM proteins in similar orientations.

FN matrix assembly is initiated by binding of FN to α5β1 integrin, a transmembrane receptor that links it to the cytoskeleton (Campbell and Humphries, 2011). Integrins cluster together to form adhesion complexes, which promote further interactions between bound FN dimers and lead to fibril formation. While a large body of work has delineated the stepwise process of FN matrix assembly (Singh *et al.*, 2010; Schwarzbauer and DeSimone, 2011), how cells assemble fibrils in a particular organization and orientation is less well understood. Previous studies have demonstrated that cells can form aligned ECM fibrils in vitro when oriented using patterned or grooved surfaces (Wang *et al.*, 2003; Sarkar *et al.*, 2005; Kim *et al.*, 2013; Singh *et al.*, 2014). Cells can remodel and reorganize established ECM fibrils by exerting contractile forces, as has been shown for a wide variety of cell types, such as osteoblast, epithelial, endothelial, and stromal cells, and contexts, such as cancer, collective migration, and tissue morphogenesis (Provenzano *et al.*, 2006; Sivakumar *et al.*, 2006; Cook *et al.*, 2017; Piotrowski-Daspit *et al.*, 2017; Davidson *et al.*, 2019; Malandrino *et al.*, 2019). Assessments of matrix configuration in these studies, however, were performed on established ECMs after fibril assembly had been completed. Whether alignment is determined at a specific step in the assembly process or by postassembly remodeling of unaligned fibrils has not been discovered.

In this study, we investigated the steps of FN assembly in a cell culture model to elucidate the process of aligned ECM formation. Microscopy and quantitative image analysis reveal initiation of aligned assembly at FN matrix assembly sites and show a previously unknown association between matrix assembly sites and another FN assembly structure, the fibrillar adhesion. We detected an association between the distribution of FN matrix assembly sites and cell elongation but found that distribution could be manipulated independent of elongation by chemical or mechanical cues. Our results lead to the conclusion that the ultimate orientation of FN fibrils is determined by the alignment and distribution of matrix assembly sites that form during the initial stages of cell–FN interactions.

RESULTS

Assessment of aligned fibronectin matrix assembly using a cell culture system

To investigate how ECM alignment is established, we used WI-38 human lung fibroblasts that assemble FN fibrils into highly aligned parallel arrays in culture (Figure 1A). Quantification of FN fibril alignment within a dense WI-38 cell matrix by fast Fourier transform (FFT) analysis shows a pixel intensity peak at 90°, indicating that fibrils within the matrix are organized in a single principal orientation (Figure 1B). Many of the subsequent experiments were performed with cells grown on a FN-coated substrate. We found that fibril organization and FFT results did not change when cells were grown on a FN coat (unpublished data). To confirm that the fibril alignment was inherent within the stable FN matrix, and not dependent on the presence of cells, we performed immunofluorescence and FFT analyses after cell removal by a decellularization procedure. Immunofluorescence images showed that FN fibrils remain aligned after decellularization (Figure 1A), and this was further confirmed by FFT analysis, which showed that the cell-free matrix retained its aligned orientation (Figure 1B). In fact, full-width at half maximum (FWHM) calculation indicates that the cell-free matrix is more aligned than the matrix with cells, since it has a lower FWHM value (Figure 1C). Together, these data establish that WI-38 fibroblasts assemble a highly aligned FN matrix.

Differences in initiation of fibronectin assembly for aligned and unaligned matrices

The early stages of FN matrix assembly were analyzed to determine when alignment of FN-based structures was first detected. Matrix assembly sites are a subset of integrin-mediated adhesions where a substrate-adsorbed FN dimer bound to α5β1 integrin undergoes conformational changes, exposing binding sites that interact with additional FN via its assembly domain (McKeown-Longo and Mosher, 1985; Singh *et al.*, 2010). These sites are the earliest observable structures of FN assembly and can be detected within 30 min after fibroblasts are plated onto a FN-coated surface (Christopher *et al.*, 1997). Initiation of FN fibrillogenesis was visualized with a matrix assembly site assay, where a biotinylated fragment of FN (70 kD) containing the assembly domain was added to culture medium and, after binding to conformationally changed FN on the substrate, was detected with fluorescent streptavidin (Figure 2A). Initially, WI-38 fibroblasts have matrix assembly sites all around the cell circumference (Figure 2B, 1 h). Matrix assembly sites redistribute into localized patches concomitant with cell shape changes and, by 4 h, bound 70 kD was often oriented in parallel arrays at the ends of elongated WI-38 cells (Figure 2B, 4 h, arrows). Polarized localization of matrix assembly sites was observed on individual WI-38 cells and did not require cell–cell contact. For comparison, we analyzed NIH 3T3 fibroblasts, which produce and assemble FN at levels similar to those for WI-38 cells (unpublished data), but assemble an unaligned fibrillar matrix with significant branching and a meshwork organization (Supplemental Figure S1). Matrix assembly sites were localized at cell projections around the cell periphery at both 1 and 4 h (Figure 2B, arrows).

To quantitatively characterize matrix assembly site orientations within individual cells, we utilized the ImageJ software package OrientationJ (Rezakhaniha *et al.*, 2012; Puspoki *et al.*, 2016). OrientationJ creates a visual representation of the orientation of structures within an image as well as a histogram of the distribution of orientations (Figure 2B; Supplemental Figure S2). Quantitative analysis of matrix assembly site orientations revealed that WI-38 matrix assembly sites were parallel to one another and had a preferred orientation with the long axis of the cell, indicated by the peak at 0° (Figure 2C). In contrast, matrix assembly sites made by NIH 3T3 cells had no particular orientation (Figure 2C). Interestingly, the matrix assembly site orientation of each cell type matches the orientation of its established FN matrix, aligned WI-38 fibrils versus unaligned NIH 3T3 fibrils.

To compare the distributions of matrix assembly sites between WI-38 and NIH 3T3 cells, we oriented each cell with its long axis horizontal, divided each cell into thirds, and scored each third for the presence of matrix assembly sites (Supplemental Figure S3).

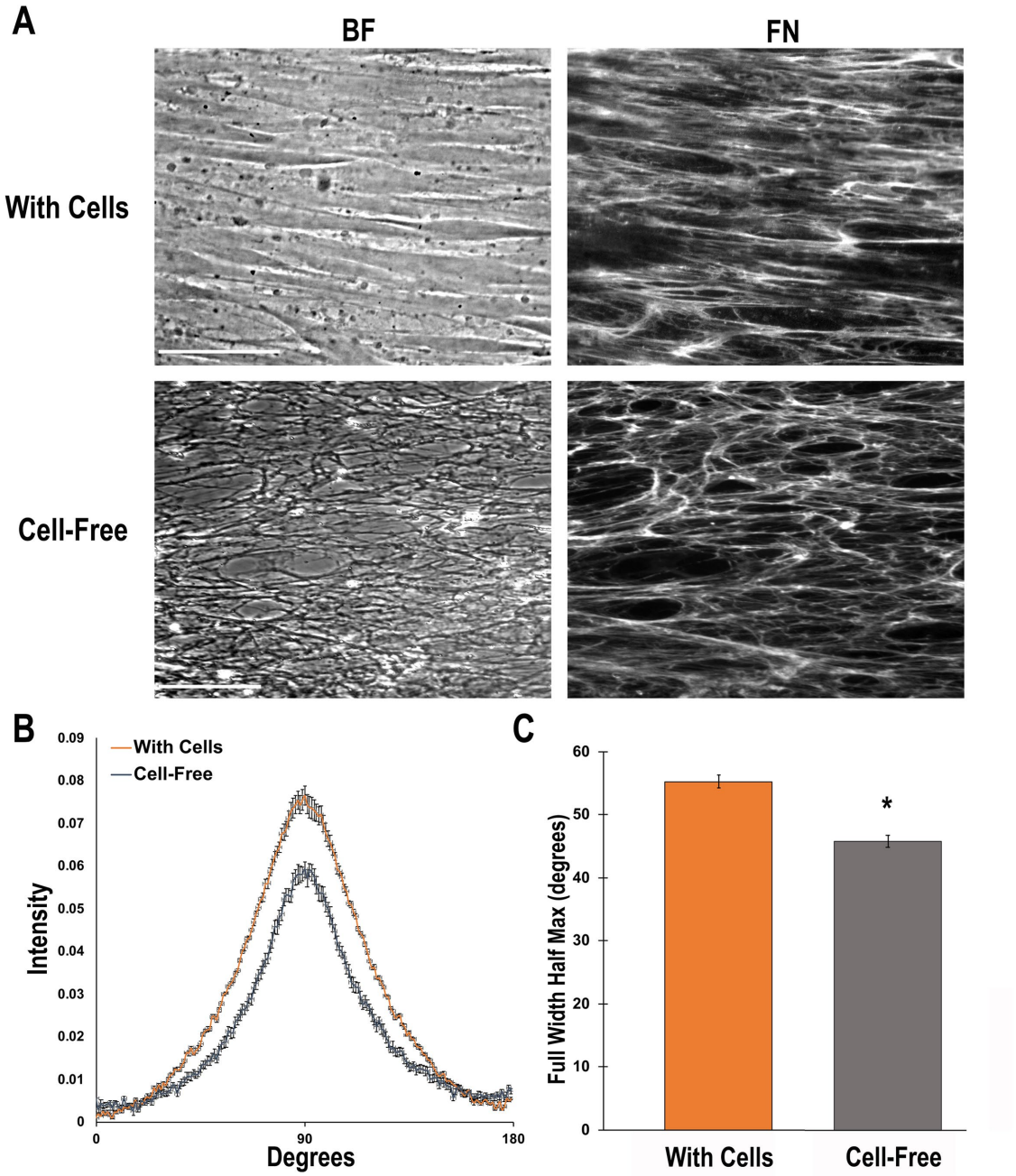

FIGURE 1: WI-38 fibroblasts assemble an aligned fibronectin (FN) matrix. (A) WI-38 cells were grown to confluence, as shown in the phase images (brightfield, BF), on glass coverslips. Samples were stained with R457 anti-FN antiserum after 3 d in culture (with cells) or monolayers were decellularized after 7 d prior fixing and staining (cell-free). Scale bar = 50 μm. (B) FN fibril orientations were quantified by FFT analysis (with cells in orange and cell-free in gray). (C) Average full-width at half maximum (FWHM) values for each pixel intensity curve of with cells (orange) and cell-free (gray) FN matrices were calculated. Error bars show the average of five curves ± standard error. * $p < 0.05$.

This analysis segregated cells into two populations: "nonpolarized," where matrix assembly sites were present in all three cell sections, and "polarized," where matrix assembly sites were absent in the middle section of the cell (Supplemental Figure S3). At 4 h after plating, 35% of WI-38 cells had polarized matrix assembly site localization with no sites in the middle section, while only 3% of NIH 3T3 cells showed polarized distributions (Figure 2D). These results show a difference in the distributions of matrix assembly sites between cells that assemble a meshwork of FN fibrils and those that assemble aligned fibrils.

Progression of matrix assembly sites into fibrillar adhesions

Fibrillar adhesions are protein complexes that organize FN into fibrils by translocation of α5β1 integrins, bound to FN, along actin filaments toward the center of the cell (Pankov *et al.*, 2000; Zamir *et al.*, 2000). Both matrix assembly sites and fibrillar adhesions are used for an evaluation of FN fibril formation, but at different times after cell adhesion, with matrix assembly sites usually identified between 15 min and 4 h after plating, while fibrillar adhesions develop between 4 and 24 h on FN. We hypothesized that matrix assembly sites mature over time into fibrillar adhesions and developed a

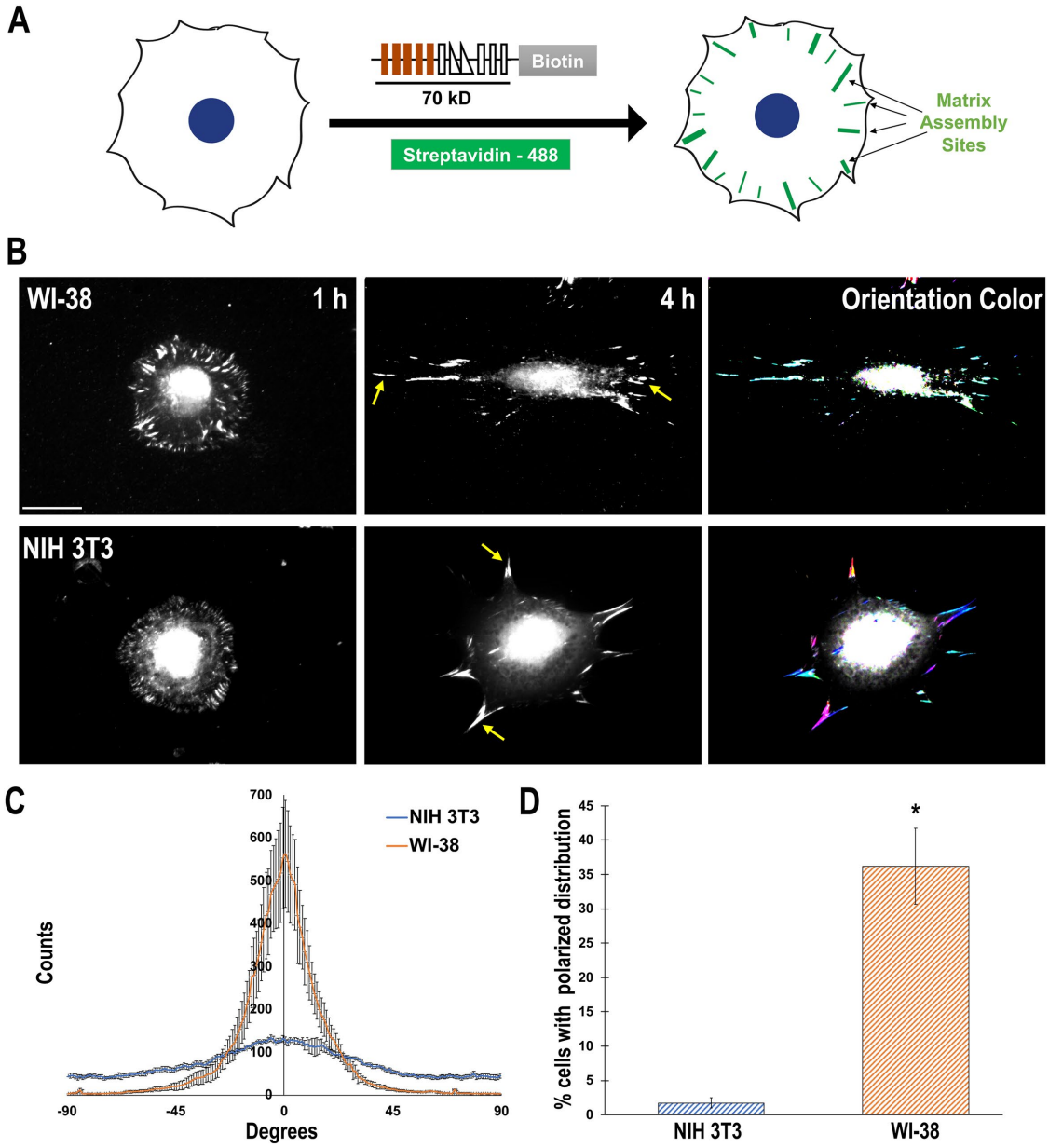

FIGURE 2: WI-38 fibroblasts develop a polarized distribution of matrix assembly sites. (A) Schematic of matrix assembly site assay. The 70 kD fragment containing the N-terminal assembly domain (orange) of FN was tagged with biotin and added to cell culture medium. 70 kD–biotin bound at matrix assembly sites was detected with streptavidin-488. (B) WI-38 (upper panels) or NIH 3T3 fibroblasts (lower panels) were allowed to spread on a FN-coated surface for the indicated times. 70 kD–biotin was added to the medium and 1 h later cells were fixed and probed with streptavidin-488. Examples of matrix assembly sites are indicated by yellow arrows. Individual matrix assembly site orientations are encoded in color in the right panel; matrix assembly sites with similar orientations are colored in the same hue (aqua for the WI-38 cell matrix assembly sites). Scale bar = 20 μm. (C) Matrix assembly site orientations were quantified for NIH 3T3 (blue) and WI-38 (orange) fibroblasts after 4 h on FN, where individual matrix assembly site orientations were calculated for individual cells using OrientationJ, averaged across cells (WI-38 $n = 27$, NIH 3T3 $n = 36$), and plotted from –90° to 90°. The orientation 0° is set to the horizontal axis of the image plane. Error bars show ± SEM of three (WI-38) or four (NIH 3T3) independent experiments. (D) The average percentage of total cells with a polarized matrix assembly site distribution at 4 h was calculated for WI-38 (orange, $n = 233$) and NIH 3T3 (blue, $n = 285$) fibroblasts. Error bars show ± SEM of three independent experiments. * $p < 0.05$, unpaired t test.

live-imaging matrix assembly site assay with total internal reflection fluorescence (TIRF) microscopy to follow these structures. We utilized preosteoblasts stably expressing RFP-tensin, a protein specifically localized to fibrillar adhesions; these cells assemble a meshwork FN matrix similar in structure to NIH 3T3 fibroblasts (Supplemental Figure S4A). Live imaging revealed that tensin colocalized with sites of matrix assembly at the cell periphery, and over time extended inward toward the cell center in fibrillar adhesions detected between 5 and 8 h (Supplemental Figure S4B). Tensin-positive fibrillar adhesions were also colocalized with matrix assembly sites in WI-38 cells (Figure 3A). The coincidence of the matrix assembly site and fibrillar adhesion peaks at 0° shows that the two

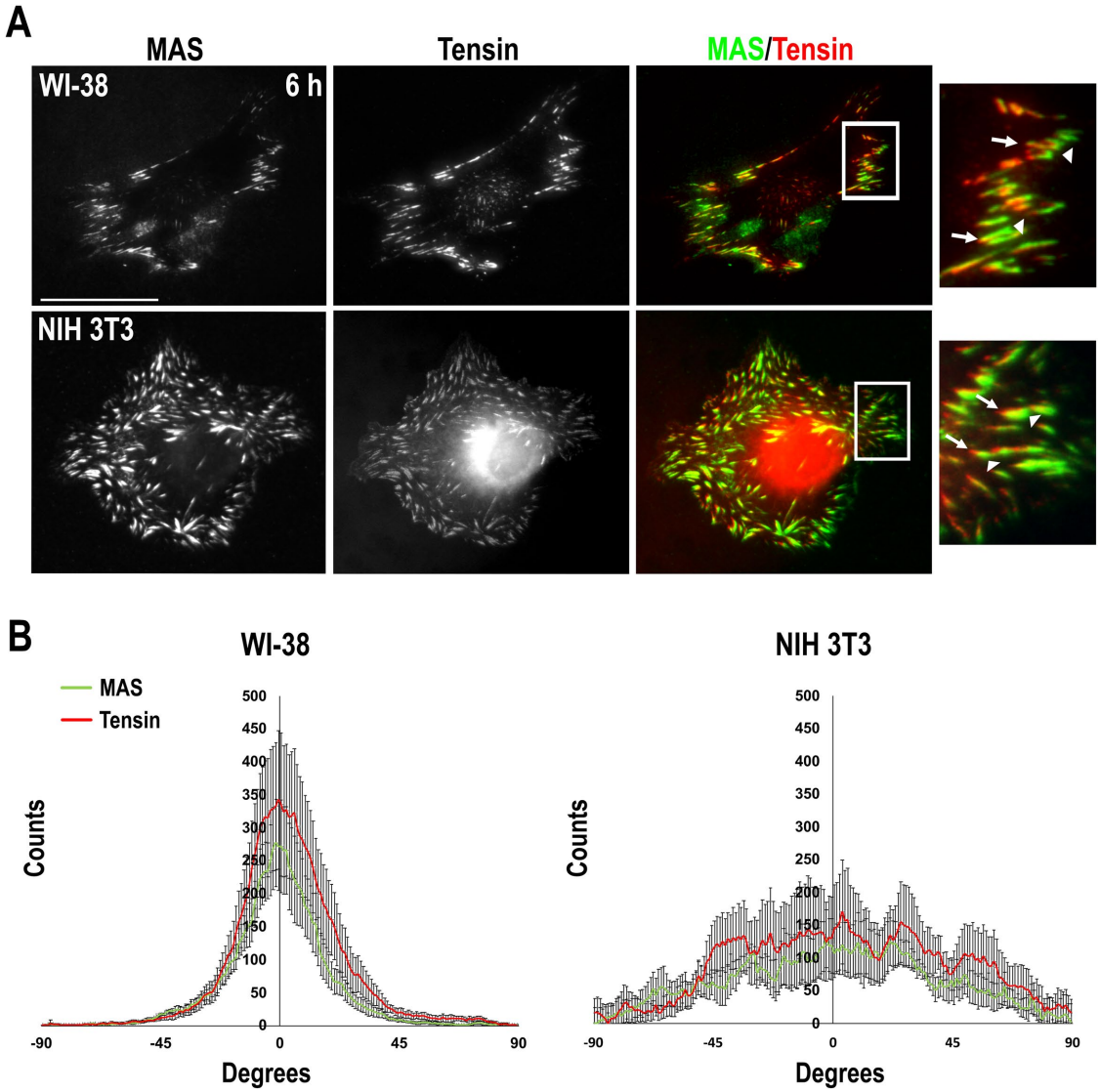

FIGURE 3: Progression of matrix assembly sites into fibrillar adhesions. (A) WI-38 fibroblasts and NIH 3T3 fibroblasts expressing fluorescently tagged tensin were plated on a FN-coated surface and 70 kD–biotin was added after 5 h. Cells were fixed 1 h later. WI-38 fibroblasts were immunostained for tensin (red, white arrow in inset) and both fibroblast cell lines were probed with streptavidin-488 (MAS, green, white arrowhead). Scale bar = 20 μm. WI-38 cells were imaged using TIRF microscopy while NIH 3T3 cells were imaged using epifluorescence. (B) The orientations of matrix assembly sites (MAS, green) and fibrillar adhesions (Tensin, red) from A were quantified by OrientationJ. Distributions were calculated for individual WI-38 ($n = 28$) or NIH 3T3 ($n = 13$) fibroblasts and then averaged. Error bars show ± SEM of three independent experiments.

structures shared a single predominant orientation angle parallel to the long axis of the cell across the entire cell body (Figure 3B). NIH 3T3 fibroblasts were analyzed over a broader time frame and in all cases showed progression of matrix assembly sites into tensin-positive fibrillar adhesions (Figure 3A; Supplemental Figure S5), but with no predominant orientation (Figure 3B). Taken together, the extension of matrix assembly sites into tensin-positive fibrillar adhesions across all three cell lines indicates that the association of these structures is a general phenomenon in ECM-assembling cells.

To determine the connection between the orientation of matrix assembly sites and fibrillar adhesions and the formation of aligned matrix fibrils, we examined FN fibril assembly by WI-38 cells over several days. As observed at earlier times, at 12 h after plating, matrix assembly sites and fibrillar adhesions were associated at cell ends and in similar orientations across the cell (Figure 4Aa). Aligned FN fibrils were extended between neighboring fibroblasts (Figure 4Ab). FWHM values calculated from FFT analyses confirm that bound 70 kD, tensin, and FN were all organized in the same predominant orientation (Figure 4B, 12 h). Coalignment of tensin and FN fibrils across groups of WI-38 cells was also observed at 24 h and 48 h (Figure 4A, c and d). FWHM values were not significantly different within and across timepoints (Figure 4B), indicating that the alignment of these molecular structures is maintained over time. The coorientation of matrix assembly sites, fibrillar adhesions, and FN fibrils at 12 h and the maintenance of the alignment of tensin and FN throughout matrix assembly shows that the polarized distribution of parallel matrix assembly sites observed early in FN fibrillogenesis results in the formation of aligned FN fibrils. Overall, we conclude that matrix assembly site alignment determines the subsequent alignment of fibrillar adhesions, and thus ultimately of FN fibrils.

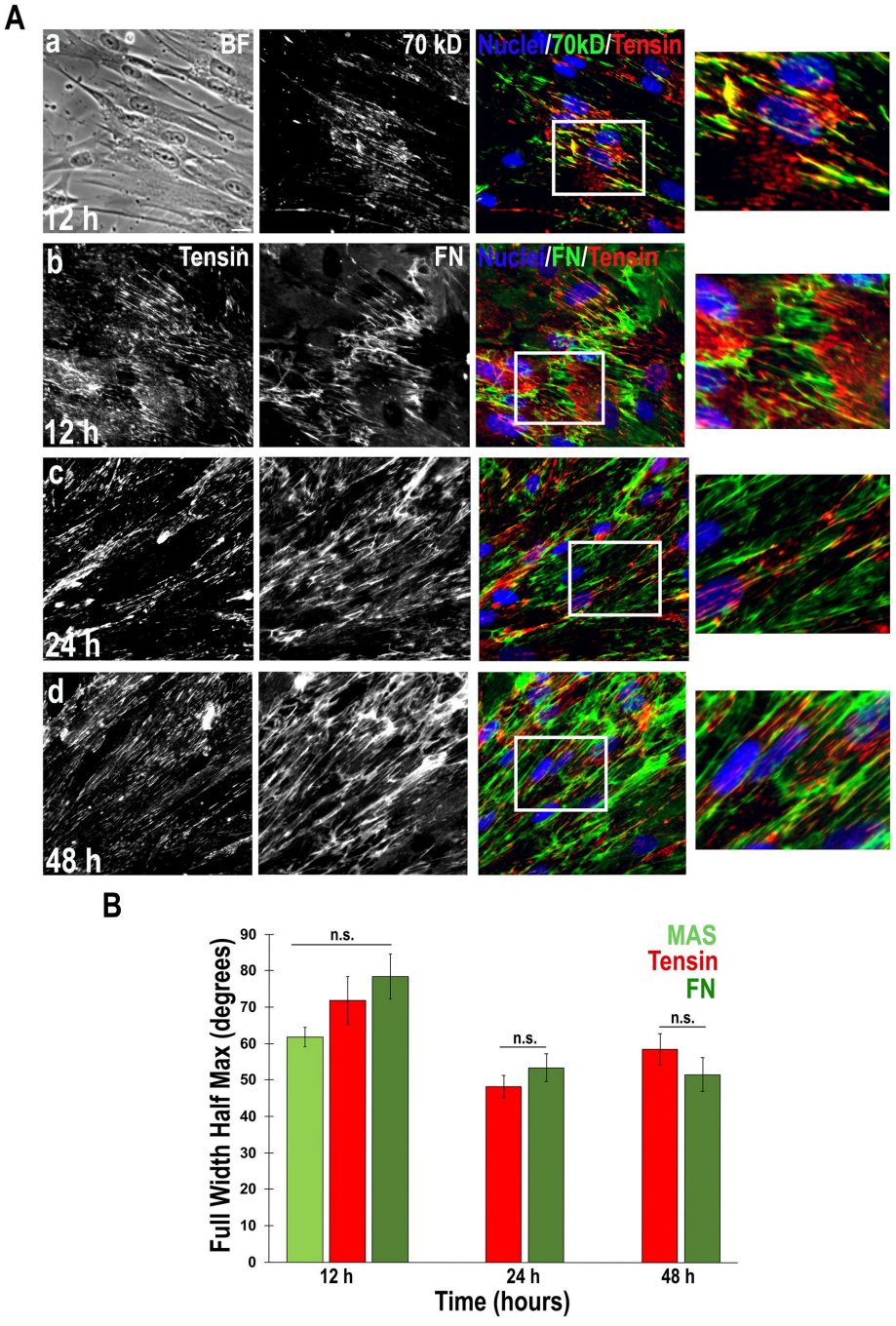

FIGURE 4: Coorientation of matrix assembly sites, fibrillar adhesions, and FN fibrils is maintained over time. (A) WI-38 fibroblasts were plated on a FN-coated surface with exogenous FN added to the medium in order to allow better visualization of FN fibers at earlier timepoints. 70 kD–biotin was added and a matrix assembly site assay was performed 1 h before fixation for (a). Cells were fixed at the indicated time points, permeabilized, immunostained for tensin (red), costained with DAPI (blue), and probed with either streptavidin-488 (green, a) or hFN7.1 anti-FN antibody (green, b, c, and d). Boxed insets are shown enlarged at the right. (B) Average FWHM values were calculated for five random fields of view at each time point. Error bars show the average of five curves ± standard error. A one-way ANOVA determined that the differences in FWHM values within and across timepoints were not significant ($p = 0.14$).

Relationship between matrix assembly site distributions and cell aspect ratios

As matrix assembly sites are being assembled, WI-38 cells take on a more elongated shape than NIH 3T3 cells. WI-38 fibroblasts have an average aspect ratio of 2.88 after 4 h on a surface coated with 10 µg/ml FN (Figure 5, A and B). By 24 h, these cells were further elongated (average aspect ratio = 4.38), with 73% of cells having an aspect ratio >3. To visualize the relationship between shape and matrix assembly site distributions, a histogram was generated that shows the proportions of polarized and nonpolarized matrix assembly sites binned by cell aspect ratio (Figure 5C). The majority of NIH 3T3 cells (>90%) had an aspect ratio less than 2 and a nonpolarized distribution of matrix assembly sites. WI-38 cells, however, had a wider range of aspect ratios and, interestingly, the proportion of cells with polarized matrix assembly sites increased significantly with aspect ratio (Figure 5C).

A functional connection between polarized matrix assembly sites and higher cell aspect ratios suggests that increasing the aspect ratios of NIH 3T3 cells should redistribute the matrix assembly sites. Micrometer-scale patterned substrates have been used to control cell shapes (Thery *et al.*, 2006; Thery, 2010; Donnelly *et al.*, 2013) and to direct cell and ECM orientations (Singh *et al.*, 2014). We designed a substrate of FN micropatterns to direct NIH 3T3 cell adhesion and spreading within 30-µm stripes of FN alternating with non–cell adhesive bovine serum albumin (BSA) protein. NIH 3T3 cells attached preferentially to the FN-coated stripes and became significantly more elongated (average aspect ratio = 2.9) than the rounder cells on the unpatterned FN-coated control surface (average aspect ratio = 1.6; Figure 6, A and B). On the stripes, cells developed a polarized distribution of matrix assembly sites, in contrast to NIH 3T3 cells on control surfaces, where the majority had matrix assembly sites distributed around the periphery (Figure 6A). At aspect ratios ≤3, the localization of most of the matrix assembly sites was not polarized, but the distribution became predominantly polarized when the aspect ratio was >3 (Figure 6C). These results demonstrate that environmental cues can increase the proportion of polarized matrix assembly sites.

To test the correlation between matrix assembly site distribution and aspect ratio, we performed a binary logistic regression analysis to model the probability that cells with a certain aspect ratio will have polarized matrix assembly sites. The regression analysis determined that a cell with an aspect ratio of 3.1 was as likely to have a nonpolarized distribution as a polarized distribution. Cells with an aspect ratio <3.1 were assigned a nonpolarized distribution and those >3.1 were assigned a polarized distribution. These assignments had an overall accuracy of 80%, with 151 matrix assembly site distributions correctly

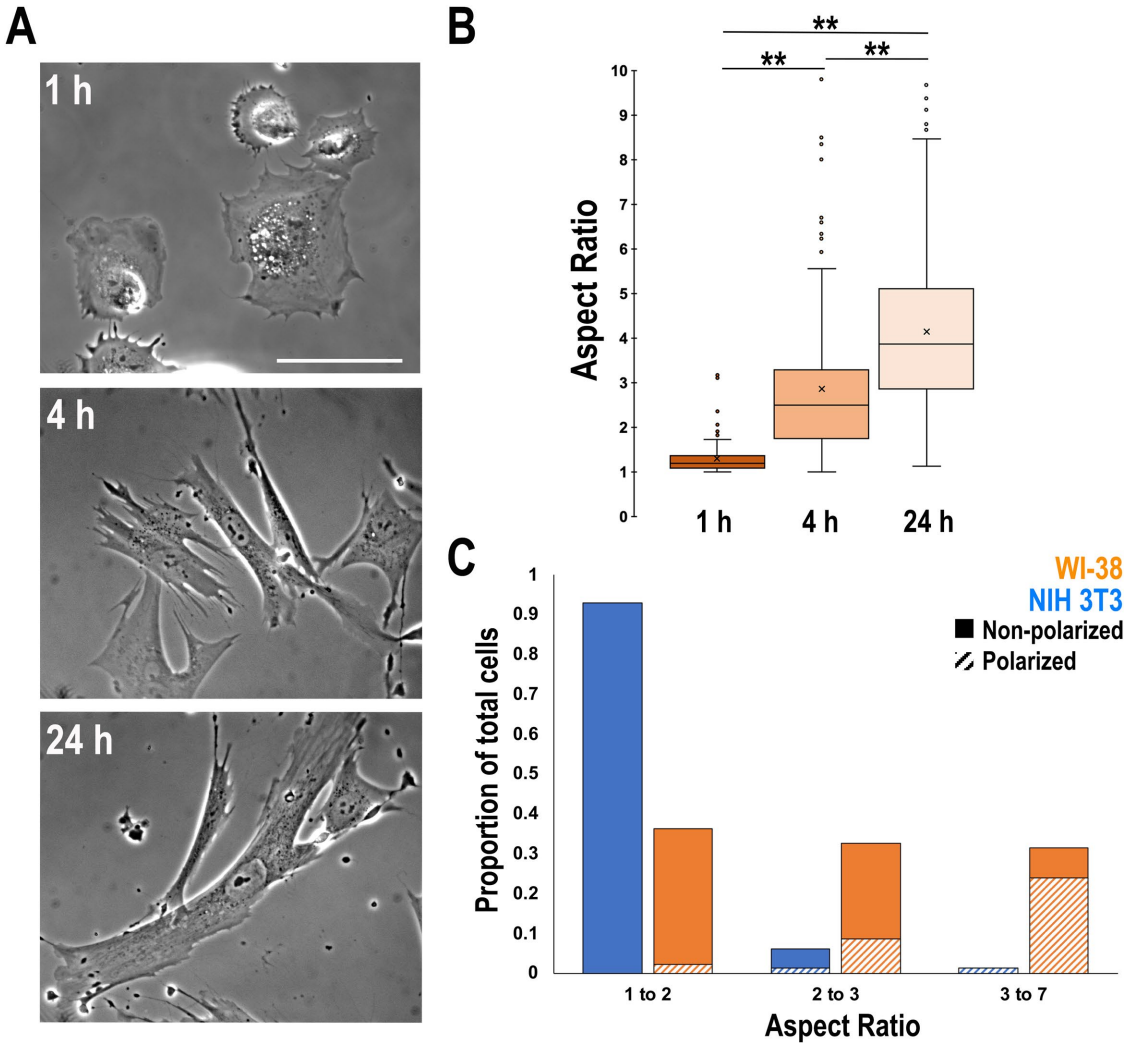

FIGURE 5: Elongation of WI-38 cells on FN. (A) WI-38 cell shape on a FN-coated surface was monitored over time using phase microscopy. Representative phase images of a single field of view are shown for each time point (1, 4, and 24 h). Scale bar = 50 μm. (B) Cell aspect ratios were determined at the indicated time points, $n > 140$ cells per time point across three independent experiments. A one-way analysis of variance with a post hoc Tukey test showed that cell aspect ratios differed significantly between all three time points (** $p < 0.0001$). (C) Cells were binned by aspect ratio and the proportion of total cells with nonpolarized (solid) or polarized (cross-hatched) matrix assembly sites were plotted for WI-38 (orange, $n = 233$) and NIH 3T3 (blue, $n = 285$) fibroblasts at 4 h. A one-way analysis of variance across three independent experiments determined that the percentage of WI-38 fibroblasts with polarized matrix assembly sites varied significantly with cell aspect ratio. Post hoc Tukey tests showed significant differences between 1 to 2 vs. 3 to 7 ($p = 0.003$) and 2 to 3 vs. 3 to 7 ($p = 0.02$) aspect ratio groups.

assigned out of 189 total cells (Supplemental Figure S6), supporting a correlation between matrix assembly site distribution and cell elongation. The analysis was effective at linking nonpolarized matrix assembly sites with aspect ratios <3.1 (90% accuracy). However, 40% of cells with polarized matrix assembly sites actually had an aspect ratio <3.1, giving 60% accuracy. This indicates that matrix assembly site polarization may arise before cell elongation and that matrix assembly site polarity is not determined solely by cell elongation.

Conclusions from the logistic regression analysis are supported by results from examining the initiation of FN fibril formation during mechanical stretch. Cells are mechanosensitive and will reorient and undergo cytoskeletal remodeling in response to stretch (Hayakawa *et al.*, 2001; Wang *et al.*, 2004; Livne *et al.*, 2014). Matrix assembly site assays were performed with cells on stretchable substrates. NIH 3T3 cells on FN-coated PDMS membranes were either stretched in 1-mm steps every 15 min for an hour and held for an additional 2.5 h or cultured without stretching for the entire 4-h period (Figure 7A). Cells were slightly elongated in the uniaxial stretch direction (average aspect ratio = 1.9) compared with unstretched controls (average aspect ratio = 1.3; Figure 7, B and C). Matrix assembly sites for cells in the rest condition were located all around the cell periphery in nonpolarized distributions (Figure 7, B and D). In contrast, cells that had been stretched had an increased incidence of polarized matrix assembly sites, with FN fibrillogenesis occurring predominantly at the cell ends (Figure 7, B and D). Interestingly, in contrast to NIH 3T3 cells on micropatterns, stretched cells had a lower average aspect ratio (1.9 versus 2.9), yet showed a higher incidence of polarized matrix assembly sites when the aspect ratio was <3. Specifically, 90% of stretched NIH 3T3 cells with polarized matrix assembly sites had an aspect ratio <3 (compare Figures 6C and 7D), compared with only 30% for NIH 3T3 cells on FN patterns and 32% for WI-38 cells

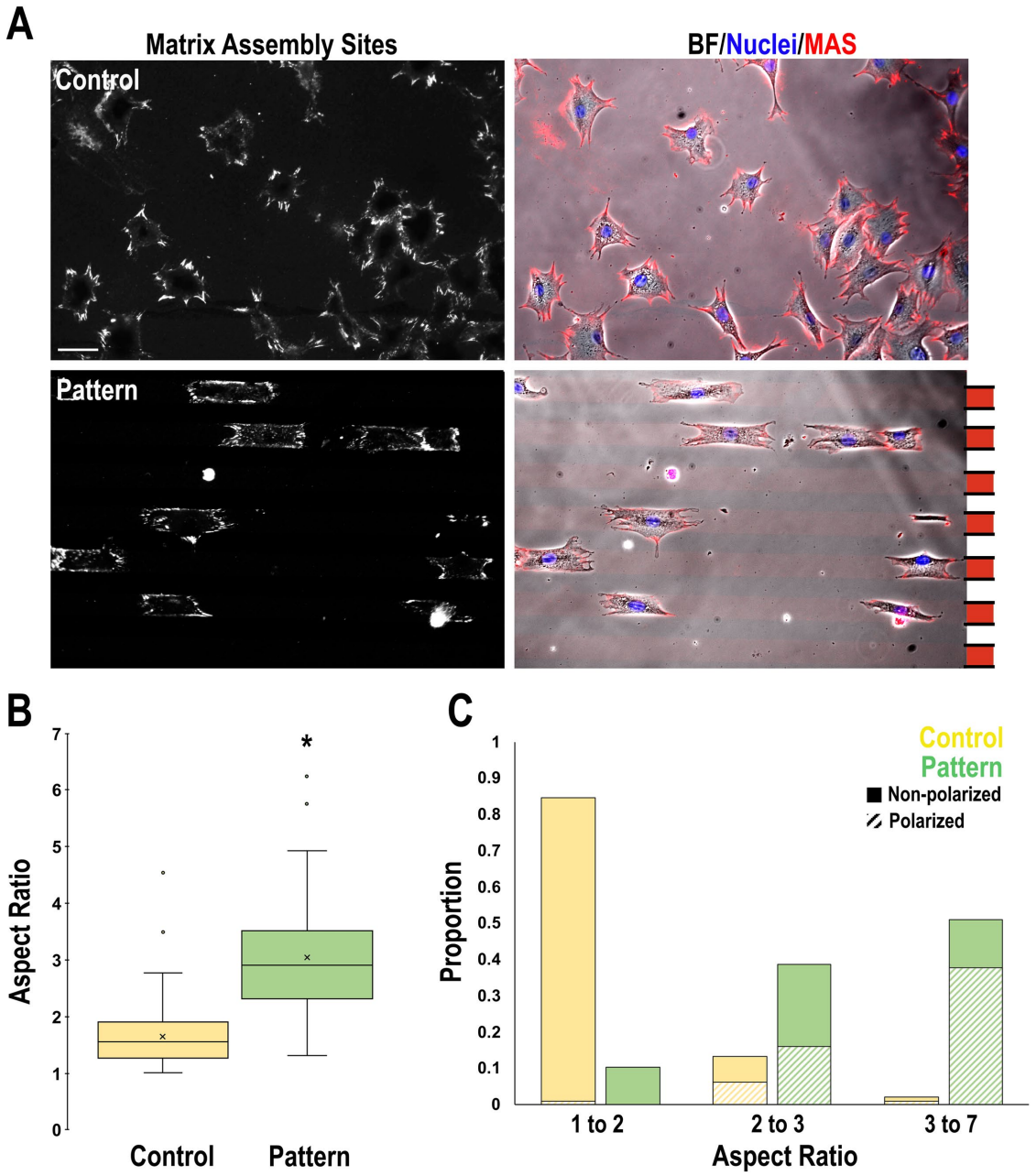

FIGURE 6: Matrix assembly site distributions of NIH 3T3 cells on FN-striped micropatterns. (A) Cells were seeded onto a surface with 30 μm–wide FN stripes and intervening 30 μm–wide BSA stripes (pattern) or onto an unpatterned FN-coated surface (control). Matrix assembly site (MAS) distributions were assayed after 4 h. Brightfield (BF), DAPI (blue, nuclei), and MAS signals are merged in the right-hand images. Scale bar = 50 μm. (B) Aspect ratios for cells on micropatterns (green) and FN-coated glass (yellow) are plotted as in Figure 5B. * $p < 0.05$, unpaired t test. (C) The proportion of cells with polarized and nonpolarized matrix assembly sites binned by cell aspect ratio is graphed, as in Figure 5C, for cells on FN micropatterns (green) or FN-coated control surfaces (yellow). A one-way analysis of variance with a post hoc Tukey test showed that the percentage of cells on FN micropatterns with polarized distributions differed significantly for 1 to 2 vs. 3 to 7 aspect ratio groups ($p = 0.02$). $n > 95$ cells across two2 independent experiments.

on a FN coat. This observation supports the idea that polarized matrix assembly site distribution may be independent of cell elongation and that it is enhanced by mechanical cues.

Control of matrix assembly site distributions by TGF-β1

Cell–FN interactions and FN matrix assembly depend on cell contractility mechanisms mediated by actomyosin (Zhang *et al.*, 1994; Zhong *et al.*, 1998). TGF-β1 treatment is known to increase fibroblast contractility and a spindle-shaped morphology (Tomasek *et al.*, 2002; Desai *et al.*, 2014). Analysis of FN matrix and actin stress fiber organization revealed that treatment of NIH 3T3 fibroblasts with TGF-β1 induced an elongated morphology at confluence and assembly of locally aligned FN fibrils as compared with vehicle-treated fibroblasts, which assembled a meshwork matrix (Figure 8A).

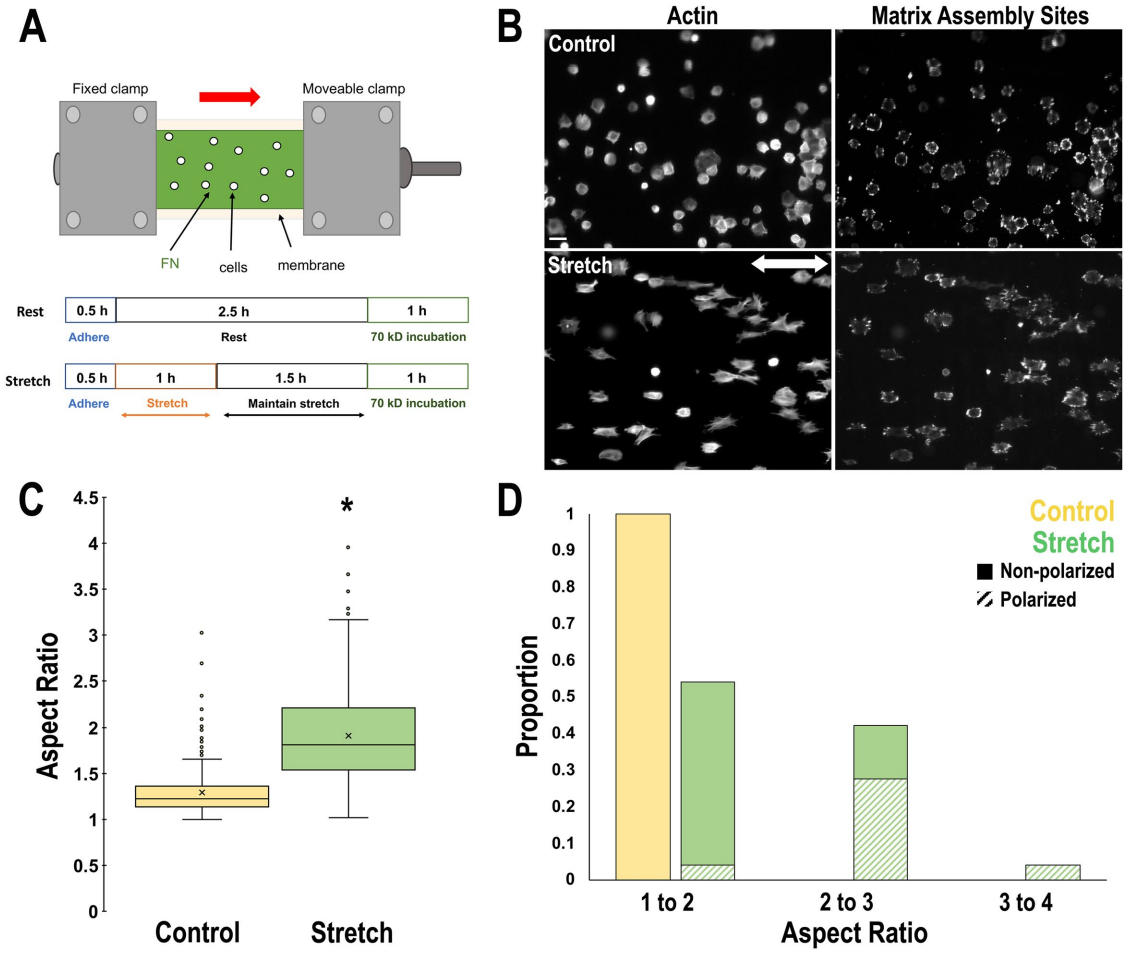

FIGURE 7: The effects of uniaxial static stretch on the distribution of NIH 3T3 cell matrix assembly sites. (A) The diagram shows the experimental design. NIH 3T3 fibroblasts were seeded onto a FN-coated PDMS membrane. After 30 min, cells were subjected to two periods of uniaxial static stretch or were allowed to rest for the indicated times. 70 kD–biotin was added to the medium and after 1 h, cells were fixed and stained. (B) Cells were costained with fluorescent streptavidin and phalloidin to visualize cells on an opaque substrate. Scale bar = 50 μm. (C) Cell aspect ratios were determined for cells under stretch (green) compared with unstretched control cells (yellow; as in Figure 5B). *$p < 0.05$, unpaired t test. $n > 240$ cells per condition across two separate experiments. (D) The proportions of cells with nonpolarized or polarized matrix assembly sites, binned by cell aspect ratio (as in Figure 5C), are shown with stretch (green) or resting (yellow). A one-way analysis of variance with a post hoc Tukey test showed that the percentage of stretched cells with polarized distributions differed significantly for the 1 to 2 vs. 2 to 3 ($p = 0.04$) and 2 to 3 vs. 3 to 7 ($p = 0.04$) aspect ratio groups. $n > 90$ cells across two independent experiments.

OrientationJ analysis provides a visual representation of alignment by encoding fibrils with parallel orientations in similar colors (Figure 8A, right panels). Because TGF-β1 is known to stimulate contractility, we confirmed that TGF-β1 treatment increased NIH 3T3 contractility using a 3D FN–fibrin clot contraction assay, where clot contraction is mediated by cell binding to FN cross-linked to fibrin. TGF-β1-treated NIH 3T3 cells showed higher matrix contraction than control cells (30.5% versus 20.3%; Supplemental Figure S7A). Comparison of NIH 3T3 and WI-38 fibroblasts showed that contraction by WI-38 cells was more than double that of untreated NIH 3T3 cells (35.0% versus 16.4%; Supplemental Figure S7B). Thus, both WI-38 fibroblasts and TGF-β1-treated NIH 3T3 cells exert contractile forces that are greater than the contractility of untreated NIH 3T3 fibroblasts.

To examine the effect of TGF-β1 on the initiation of FN assembly, we performed a matrix assembly site assay. Similarly to our previous observations, we detected matrix assembly sites all around the cell periphery in untreated cells (Figure 8Ba) and found matrix assembly site distributions to be polarized in cells with aspect ratios >3 (Figure 8Bb). Interestingly, TGF-β1 treatment significantly increased polarized matrix assembly sites (Figure 8Bc). More than 90% of TGF-β1-treated cells had aspect ratios <3, yet the proportion of cells with a polarized matrix assembly site distribution increased from 7% in the control to 21% with TGF-β1 (Figure 8C). This result supports the idea that the polar localization of matrix assembly sites is independent of cell elongation. In addition to mechanical cues, our results with TGF-β show that chemical signals in the microenvironment can control the organization of matrix assembly sites and induce the alignment of FN fibrils in cells that normally assemble a meshwork ECM.

DISCUSSION

The aligned organization of ECM fibrils is critical for the proper functions of certain tissues but also contributes to disease progression.

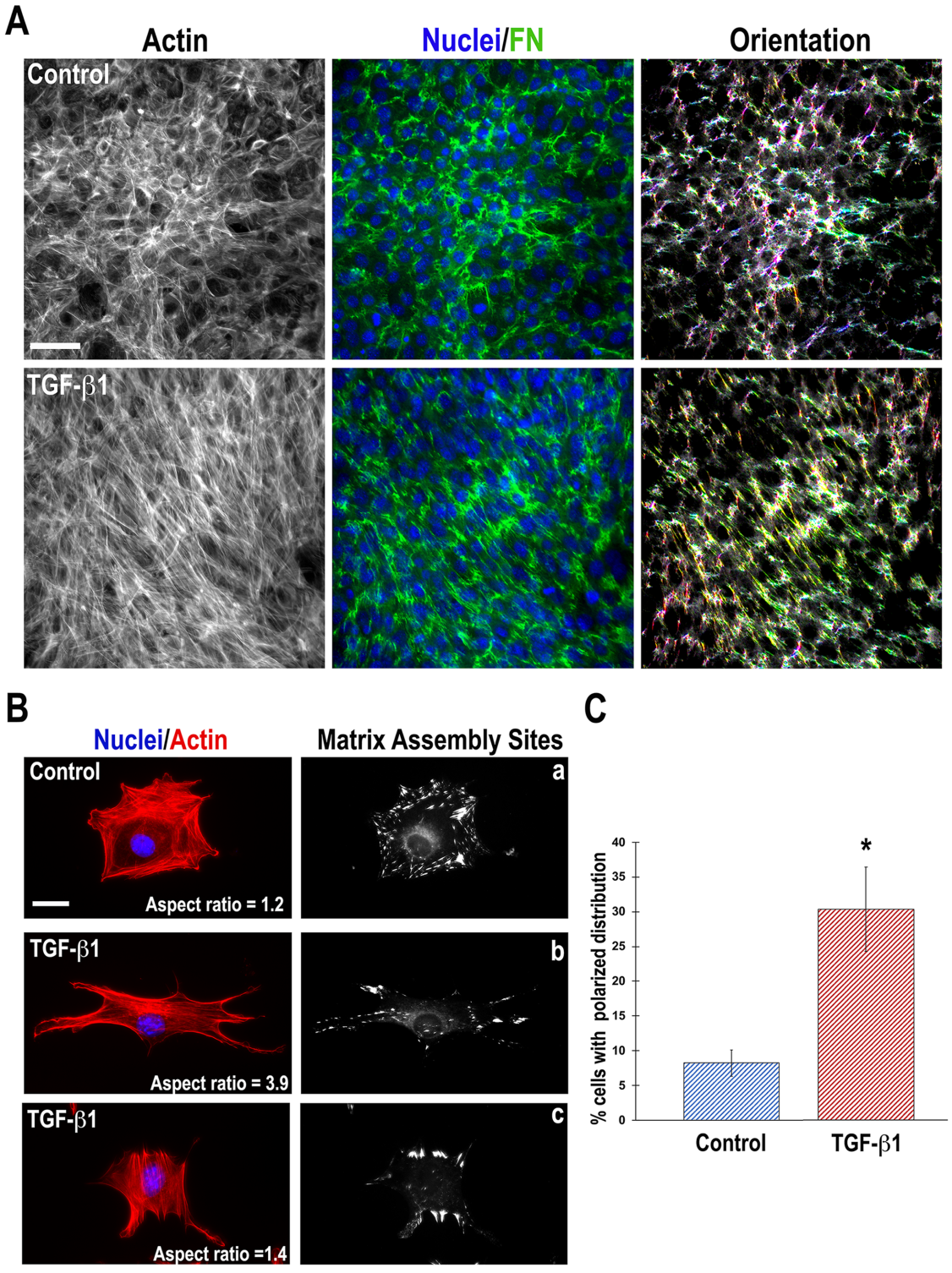

FIGURE 8: TGF-β1 induces a polarized matrix assembly site distribution and assembly of aligned FN fibrils. (A) NIH 3T3 cells were grown in complete medium containing either 10 ng/ml TGF-β1 or vehicle and fixed upon reaching confluence. Cells were immunostained with anti-FN antiserum (green), phalloidin to visualize actin (gray scale), and DAPI to detect nuclei (blue). FN fibril orientations are encoded in color in the rightmost panel; fibrils with similar orientations are colored in the same hue. (B) Matrix assembly sites were detected on NIH 3T3 cells plated on FN-coated surfaces and treated with TGF-β1 or vehicle for 6 h. Cells treated with TGF-β1 or vehicle were stained for matrix assembly sites and costained with Texas red phalloidin (red) and DAPI (blue). Representative images of cells are shown. The aspect ratio of each cell is indicated on the left images and matrix assembly site distributions are shown for the same cells (right). (C) The average percentage of total cells with a polarized matrix assembly site distribution is shown for vehicle-treated (blue, $n = 207$) and TGF-β1-treated (red, $n = 206$) cells. Matrix assembly site assay was performed as described in B. Error bars show ± SEM of three independent experiments. * $p < 0.05$, unpaired t test.

In this study, we investigated the mechanism of de novo aligned assembly of FN fibrils by fibroblasts and show that fibril alignment is determined by the distribution of matrix assembly sites formed in the initial stages of cell–FN interactions. We identified a novel association between matrix assembly sites and fibrillar adhesions, the two earliest protein complexes involved in fibril assembly. We followed the progression of FN fibril assembly from the initial formation of matrix assembly sites, through their rearrangement into polarized and oriented distributions, their development into aligned fibrillar adhesions and nascent FN fibrils, and ultimately to the formation of an aligned, insoluble FN matrix. Matrix assembly site alignment occurred as WI-38 cells were spreading into an elongated morphology. However, polarized matrix assembly site distributions could be induced in NIH 3T3 cells independent of cell elongation by mechanical or chemical stimuli. Thus, modulation of the orientation of these complexes by environmental signals is likely to contribute to the orientation of the ECM in vivo. We found that fibroblasts assembling an aligned FN matrix were more contractile than fibroblasts that assembled a meshwork matrix. Cell contractility, polarization of matrix assembly sites, and assembly of aligned FN fibrils were all induced by TGF-β. Mechanistically, growth factor stimulation during the initial stages of cell–FN interactions may provide a means to control the distribution of matrix assembly sites and to determine the alignment of the ECM during tissue development.

In our system, WI-38 cells assembled highly aligned FN fibrils de novo on an unpatterned surface. We demonstrated a correlation between WI-38 cell aspect ratio and the formation of polarized, parallel matrix assembly sites. However, results from logistic regression analysis, mechanical stretch, and TGF-β treatment indicate that the polarized organization of matrix assembly sites arises in the absence of or before elongation. Focal adhesions are mechanosensitive and transmission of mechanical signals, such as stretch, is mediated by integrin- and/or actin-binding focal adhesion components, such as talin and vinculin (Sun *et al.*, 2019). Others have shown that focal adhesions respond to uniaxial stretch by reinforcing adhesions parallel to the stretch direction and disassembling adhesions oriented perpendicular (Chen *et al.*, 2013). Because matrix assembly sites colocalize with vinculin-containing focal adhesions around the cell periphery (Christopher *et al.*, 1997), it is possible that sites oriented in the stretch direction are reinforced while FN dimers at other sites are released due to focal adhesion disassembly, resulting in a polarized distribution. Matrix assembly site polarization may arise first in nonelongated cells and subsequently direct cell elongation. Live imaging of chondrogenesis in growth plate cartilage explants has shown that polarized cell behaviors, such as chondrocyte rearrangement, are independent of physical indicators of cell polarity such as cell shape (Romereim *et al.*, 2014). Additionally, reorientation of actin stress fibers has been observed before cell elongation (Greiner *et al.*, 2013). Stress fibers are linked to focal adhesions and sites of matrix assembly (Livne and Geiger, 2016). Perhaps it is the polarization of matrix assembly sites that then generates stress fiber reorientation and induces changes in cell shape and elongation.

Fibronectin matrix assembly, regardless of matrix organization, requires cell contractility, and disruption of actin filaments by cytochalasin D prevents formation of matrix assembly sites (Zhang *et al.*, 1994; Christopher *et al.*, 1997; Zhong *et al.*, 1998). Integrin activation occurs at sites of matrix assembly and has been shown to contribute to aligned FN fibril formation by cancer fibroblasts (Erdogan *et al.*, 2017). Indeed, we have observed that kindlin-2, an adaptor protein that binds to the cytoplasmic tail of β1 integrin and is involved in integrin activation (Kloeker *et al.*, 2004; Theodosiou *et al.*, 2016), colocalizes with matrix assembly sites in WI-38 fibroblasts (C.M.G., unpublished observations). It is possible that local fluctuations in these regulators of integrin activity may strengthen some matrix assembly sites and initiate the formation of a polarized distribution through positive feedback mechanisms.

In vivo, cells are continually exposed to microenvironmental cues, both biochemical and physical, that affect their behavior. Our work shows that ECM organization is established in the early stages of cells binding to ECM but can be altered or reinforced by physical (micropatterns) or mechanical (stretch) signals. These findings indicate that in a tissue microenvironment with established alignment cues, such as collagen fibers in the tendon (Birk and Trelstad, 1986) or blood vessel wall (Heidari *et al.*, 2015), naive cells are directed to assemble aligned ECM through contact guidance. For example, after cell division, this guidance is likely important for directing oriented reattachment of daughter cells.

Different mechanisms are probably at play in microenvironments lacking preexisting alignment cues, and the signals that instruct aligned matrix formation during tissue development may differ from those utilized for maintenance of tissue architecture or under pathological conditions. In the absence of preexisting cues, aligned matrix assembly may instead depend on chemical signals such as those from TGF-β to induce cells and tissues to adapt to new conditions, where aligned matrix or an elongated cell shape are needed for appropriate function or structure. TGF-β isoforms are highly expressed during tendon development and healing (Chen *et al.*, 2008; Liu *et al.*, 2012), and disruption of TGF-β signaling during mouse development results in loss of most tendons and ligaments (Pryce *et al.*, 2009). TGF-β isoforms also promote matrix alignment in a 3D corneal model (Karamichos *et al.*, 2011). Examination of a publicly available RNAseq dataset from Gene Expression Omnibus (GEO) revealed that WI-38 fibroblasts express several TGF-β1 pathway components at higher levels than NIH 3T3 cells (Marthandan *et al.*, 2015), which may contribute to the aligned assembly of WI-38 FN matrix. TGF-β may synergize with other mechanisms, such as mechanical stretch, to influence matrix assembly sites and cell-mediated matrix assembly. Complementary mechanisms may have context-dependent hierarchies. Understanding the different mechanisms involved in formation of aligned matrix can help inform strategies to restore aligned ECM after injury or perturb its formation under pathological conditions.

MATERIALS AND METHODS

Cell culture and reagents

NIH 3T3 mouse fibroblasts (ATCC, Manassas, VA) were maintained in DMEM (Life Technologies, Grand Island, New York) with 10% bovine calf serum (Hyclone, Logan, UT) and antibiotic/antimycotic cocktail (Corning Life Sciences, Oneonta, NY). WI-38 human lung fibroblasts (ATCC, Manassas, VA) were grown in modified Eagle's medium (MEM) containing 1% nonessential amino acids and 1 mM sodium pyruvate (all from Life Technologies, Grand Island, NY) supplemented with 10% fetal bovine serum (Hyclone, Logan, UT), 4 mM glutamine (ThermoFisher) and penn-strep (ThermoFisher). RFP-tensin preosteoblasts (a gift from Drs. Bernhard Wehrle-Haller and Daniel Bouvard; Stanchi *et al.*, 2009; Brunner *et al.*, 2011) were cultured in DMEM supplemented with 10% fetal bovine serum (Hyclone, Logan, UT) and antibiotic/antimycotic cocktail (Corning Life Sciences, Oneonta, NY). Cells were randomly tested throughout culture and found to be free of mycoplasma contamination.

Recombinant human TGF-β1 protein was solubilized in 4 mM HCL, 0.1% BSA according to the manufacturer's instructions (R&D Systems, Minneapolis, MN). Fibronectin was purified from frozen human plasma by gelatin-Sepharose affinity chromatography and

dialyzed into CAPS buffer (Wilson and Schwarzbauer, 1992). Recombinant 70 kD was generated with a baculovirus insect cell expression system (Aguirre *et al.*, 1994; Carraher and Schwarzbauer, 2013) and was biotinylated using EZ-Link sulfo-NHS-biotin (N-hydroxy sulfosuccinimidyl biotin) according to the manufacturer's instructions (ThermoFisher, 21217). Rabbit anti-fibronectin antiserum (R457; Aguirre *et al.*, 1994) diluted 1:100, hFN7.1 anti-human FN monoclonal antibody (DSHB, Iowa City, IA) diluted 1:500, and rabbit anti-tensin 1 antibody (Sigma-Aldrich) diluted to 1:200 were used for immunofluorescence. Alexa Fluor conjugated streptavidin-488 (ThermoFisher) was utilized to detect bound 70 kD–biotin. Secondary antibodies were Alexa Fluor 568-goat anti-rabbit IgG (H+L) and Alexa Fluor 488-goat anti-rabbit IgG (H+L) (Life Technologies) all diluted 1:500. DAPI was diluted 1:600 (Sigma-Aldrich), and Texas Red-X Phalloidin was diluted 1:100 (ThermoFisher, T7471). All antibodies were diluted in 2% ovalbumin in PBS.

Immunofluorescence of fibronectin matrix and matrix assembly site assay

For analysis of the matrix, 5×10^4 cells were plated onto glass coverslips in complete medium and allowed to grow to confluence. Three days postconfluence, cells were fixed with 3.7% formaldehyde in PBS and stained with R457 antiserum. For analysis of decellularized matrix, 1.5×10^5 cells were plated in complete medium and grown for 7 d. The standard Schwarzbauer lab decellularization protocol (Harris *et al.*, 2018) was used with the following modifications: an additional 15-min lysis buffer incubation and extension of the third lysis buffer incubation to 1.25 h.

Coverslips were coated overnight with 10 µg/ml human plasma FN at 4°C. For matrix assembly site assays, 1×10^4 cells/cm^2 were plated onto the FN-coated coverslips in a 24-well dish. For analysis of matrix assembly over several days, cells were plated onto FN-coated coverslips at 2.5×10^4 cells/cm^2. Cells that had not attached after 30 min on FN were removed by aspiration of medium. One hour before fixation, 10 µg/ml biotinylated 70 kD was added to the medium. Fluorescently tagged streptavidin was used at a concentration of 4 µg/ml to identify sites of bound 70 kD after fixation. For analysis of intracellular proteins (such as tensin), cells were permeabilized with 0.5% Triton X-100 (Sigma) in PBS for 15 min at room temperature.

Quantitative image analysis

To quantify cell shape, cells were outlined using phase images and FIJI software (ImageJ, NIH). The fit ellipse tool determined the major and minor axes of each cell. These measurements were used to determine cell aspect ratio, which was calculated by dividing the major axis by the minor axis. All cell aspect ratios across independent experiments were depicted in a boxplot for each condition. Boxes span the 25th to 75th percentiles, and whiskers denote the inner fences of the distribution, which are the limits the data must be within in order not to be considered outliers. The midline in the box represents the median, and the x indicates the mean. For assessment of matrix assembly site distribution across the cell, the major axis of each cell was used to divide the cell into three sections equal in length. The presence or absence of matrix assembly sites, indicated by the presence of bound 70 kD, was scored for each cell section. The plugin OrientationJ was utilized to determine the orientation of individual matrix assembly sites within a cell (Rezakhaniha *et al.*, 2012; Puspoki *et al.*, 2016). In brief, 8-bit images (60× magnification) were cropped so only a single cell was present in an image for measurement. The OrientationJ horizontal alignment tool was utilized to set the dominant orientation within an image to the horizontal axis, which allowed detection of patterns in orientation direction across multiple cells. A 2-pixel Gaussian analysis window was specified, and the Gaussian window moved across the image to calculate structure tensors for the determination of local orientations. Orientation (in degrees, which could range from -90° to +90° from the horizontal) was encoded by color in a visual representation as well as a histogram of the distribution of orientations. If the structures in an image had similar orientations, OrientationJ would encode the image structures with a similar hue and produce a histogram with a peak over the common orientation angle.

FN matrix orientation was quantified by fast Fourier transform (FFT) analysis using five cropped (1024 × 1024) eight-bit images (20× magnification). A grayscale mask was constructed as described previously (Ayres *et al.*, 2008; Huang *et al.*, 2012; Singh *et al.*, 2014) using a gradation of grayscale pixels to account for edge artifacts. Oval Profile Plugin (authored by William O'Connell) was used to determine the summed pixel intensity for each angle between 0° and 360°. Because the plot is nearly symmetrical, the radial intensity data were averaged and plotted from 0° to 180°, and then normalized to a baseline value of 0 and plotted in arbitrary units ranging from 0 to 0.10.

Fibronectin micropatterning and stretching experiments

For micropatterning experiments, a polydimethylsiloxane (PDMS) stamp approximately 1 cm by 1 cm (a gift from Daniel Cohen, Princeton University) consisting of raised lines 30 µm in width separated by microwell lines 30 µm in width was coated with 10% bovine serum albumin (BSA, Sigma-Aldrich) in dH_2O for 30 min at 37°C. Stamps were washed with dH_2O after BSA coating. Glass surfaces were plasma-cleaned using a basic benchtop plasma cleaner (PDC-32G, Harrick Plasma) on high for 1 min before stamping. Immediately after plasma cleaning, BSA-coated PDMS stamps were placed in contact with the glass surface. A 4-g weight was placed on top of the stamp to ensure contact and enhance protein transfer from the stamp to the glass. After 5 min of contact, the stamp was carefully removed, and the glass surface was immediately washed three times with PBS. The BSA-patterned glass surface was then incubated with 10 µg/ml human plasma FN overnight at 4°C. Cells were seeded on the BSA-FN micropatterns for matrix assembly site assays as described above.

For stretching experiments, a custom-designed stretch chamber (Aw *et al.*, 2016) containing a flexible 7 × 3 cm PDMS membrane (SSP-M823-005, Specialty Silicone Products) was exposed to UV light for 30 min and then coated with 50 µg/ml human plasma FN overnight at 4°C followed by washing with PBS. A sample of 5×10^4 cells were given 30 min to attach to the FN-coated PDMS, unattached cells were removed, and fresh medium was added. The PDMS membrane was stretched 2.0 mm every 15 min for a period of 1 h. Then membranes were held in a stretched position for an additional 2.5 h, during which time the matrix assembly site assay was performed as described. Quantification of cell aspect ratios for both micropatterning and stretch experiments was performed using FIJI software as described.

Epifluorescence and total internal reflection fluorescence microscopy

Coverslips were mounted using ProLong Gold Antifade Reagent (Life Technologies, Grand Island, NY). Images were captured using either a Nikon Eclipse Ti microscope equipped with a Hamamatsu C11440 ORCA-Flash 4.0 LT plus digital camera and NIS-Elements Software (Nikon, Melville, NY) or a Hamamatsu C10600 ORCA-R2 digital camera and iVision acquisition software. Images compared with one another were equivalently adjusted for brightness and contrast in FIJI for presentation in figures. All FFT or OrientationJ analyses were performed on unadjusted 8- or 16-bit images, respectively.

Total internal reflection fluorescence (TIRF) microscopy was performed on a Nikon Ti-E with a perfect focus system fitted with an Andor iXon Ultra CCD camera (Oxford Instruments). Images were captured with NIS-Elements Software. Live-cell matrix assembly site assays were performed as described above, with the following modifications: after removal of cells that had not attached by 30 min, 10 μg/ml biotinylated 70 kD biotin was added to the medium, followed by 4 μg/ml fluorescently tagged streptavidin 10 min later. Samples were then brought down to the TIRF microscope for live imaging.

Fibronectin–fibrin matrix contraction assay

Fibrin–FN matrices were prepared as described previously (Corbett and Schwarzbauer, 1999; Midwood and Schwarzbauer, 2002) by mixing components to yield the following final concentrations: 600 μg/ml human fibrinogen (BioVision Inc, Milpitas, CA), 150 mM sodium chloride, 20 mM calcium chloride, and 10 mM Tris-HCl, pH 7.4. No additional FN or Factor XIII was required for clot formation. Cells were resuspended in a 0.025 M HEPES/0.13 M NaCl solution and added to the clot components for a final concentration of 1.2×10^6 cells/ml. After thrombin addition, the mixture was quickly pipetted into BSA-coated wells and incubated at 37°C. After 30 min at 37°C, FN-depleted medium was added to the wells and clots were carefully detached from the well walls using a thin needle under a dissecting microscope. The diameter of the clot was measured over 4 h as described previously (Corbett and Schwarzbauer, 1999; Midwood and Schwarzbauer, 2002). The percentage contraction for each condition was normalized to the contraction of a clot that did not contain cells. For treatment of cells with TGF-β1, fibroblasts were grown for 24 h in medium containing 10 ng/ml recombinant TGF-β1 protein or an equivalent volume of vehicle before use in contraction assay.

Logistic regression and statistical analysis

Logistic regression analysis was performed using the Excel data analysis add-on XLSTAT. The cutoff value was set at $p = 0.50$. For all other statistical analyses, *p*-values were determined from the results of 2–4 independent experimental replicates using either Student's *t* test or one-way analysis of variance (ANOVA) with post hoc Tukey testing. Values less than 0.05 were considered to be significant.

ACKNOWLEDGMENTS

We are grateful to Wen Yih Aw and Danelle Devenport for providing the stretch chamber and to Daniel Cohen for providing PDMS stamps and sharing his micropatterning expertise. We kindly thank Berhard Wehrle-Haller and Daniel Bouvard for providing the preosteoblasts expressing RFP-tensin. We also thank Gary Laevsky, director of the Molecular Biology Confocal Microscopy Core Facility, a Nikon Center of Excellence, for his technical assistance and members of the Schwarzbauer lab for insightful discussions. This research was funded by NIAMS R01 AR073236 (to J.E.S.), a New Jersey Commission on Cancer Research (NJCCR) DFHS18PPC041 predoctoral fellowship (to C.M.G.), and a NIH T32 GM007388 predoctoral training grant to the Department of Molecular Biology at Princeton University.

REFERENCES

Aguirre KM, McCormick RJ, Schwarzbauer JE (1994). Fibronectin self-association is mediated by complementary sites within the amino-terminal one-third of the molecule. J Biol Chem 269, 27863–27868.

Aw WY, Heck BW, Joyce B, Devenport D. (2016). Transient tissue-scale deformation coordinates alignment of planar cell polarity junctions in the mammalian skin. Curr Biol 26, 2090–2100.

Ayres CE, Jha BS, Meredith H, Bowman JR, Bowlin GL, Henderson SC, Simpson DG (2008). Measuring fiber alignment in electrospun scaffolds: a user's guide to the 2D fast Fourier transform approach. J Biomater Sci Polym Ed 19, 603–621.

Birk DE, Trelstad RL (1986). Extracellular compartments in tendon morphogenesis: collagen fibril, bundle, and macroaggregate formation. J Cell Biol 103, 231–240.

Bosman FT, Stamenkovic I (2003). Functional structure and composition of the extracellular matrix. J Pathol 200, 423–428.

Brunner M, Millon-Fremillon A, Chevalier G, Nakchbandi IA, Mosher D, Block MR, Albiges-Rizo C, Bouvard D (2011). Osteoblast mineralization requires beta1 integrin/ICAP-1-dependent fibronectin deposition. J Cell Biol 194, 307–322.

Burgstaller G, Oehrle B, Gerckens M, White ES, Schiller HB, Eickelberg O (2017). The instructive extracellular matrix of the lung: basic composition and alterations in chronic lung disease. Eur Respir J 50.

Campbell ID, Humphries MJ (2011). Integrin structure, activation, and interactions. Cold Spring Harb Perspect Biol 3.

Canty EG, Starborg T, Lu Y, Humphries SM, Holmes DF, Meadows RS, Huffman A, O'Toole ET, Kadler KE (2006). Actin filaments are required for fibripositor-mediated collagen fibril alignment in tendon. J Biol Chem 281, 38592–38598.

Carraher CL, Schwarzbauer JE (2013). Regulation of matrix assembly through rigidity-dependent fibronectin conformational changes. J Biol Chem 288, 14805–14814.

Chen CH, Cao Y, Wu YF, Bais AJ, Gao JS, Tang JB (2008). Tendon healing in vivo: gene expression and production of multiple growth factors in early tendon healing period. J Hand Surg Am 33, 1834–1842.

Chen Y, Pasapera AM, Koretsky AP, Waterman CM (2013). Orientation-specific responses to sustained uniaxial stretching in focal adhesion growth and turnover. Proc Natl Acad Sci USA 110, E2352–E2361.

Christopher RA, Kowalczyk AP, McKeown-Longo PJ (1997). Localization of fibronectin matrix assembly sites on fibroblasts and endothelial cells. J Cell Sci 110 (Pt 5), 569–581.

Conklin MW, Eickhoff JC, Riching KM, Pehlke CA, Eliceiri KW, Provenzano PP, Friedl A, Keely PJ (2011). Aligned collagen is a prognostic signature for survival in human breast carcinoma. Am J Pathol 178, 1221–1232.

Cook CD, Hill AS, Guo M, Stockdale L, Papps JP, Isaacson KB, Lauffenburger DA, Griffith LG (2017). Local remodeling of synthetic extracellular matrix microenvironments by co-cultured endometrial epithelial and stromal cells enables long-term dynamic physiological function. Integr Biol (Camb) 9, 271–289.

Corbett SA, Schwarzbauer JE (1999). Requirements for alpha(5)beta(1) integrin-mediated retraction of fibronectin-fibrin matrices. J Biol Chem 274, 20943–20948.

Davidson CD, Wang WY, Zaimi I, Jayco DKP, Baker BM (2019). Cell force-mediated matrix reorganization underlies multicellular network assembly. Sci Rep 9, 12.

Desai VD, Hsia HC, Schwarzbauer JE (2014). Reversible modulation of myofibroblast differentiation in adipose-derived mesenchymal stem cells. PLoS One 9, e86865.

Donnelly PE, Jones CM, Bandini SB, Singh S, Schwartz J, Schwarzbauer JE (2013). A simple nanoscale interface directs alignment of a confluent cell layer on oxide and polymer surfaces. J Mater Chem B 1, 3553–3561.

Erdogan B, Ao M, White LM, Means AL, Brewer BM, Yang L, Washington MK, Shi C, Franco OE, Weaver AM, *et al.* (2017). Cancer-associated fibroblasts promote directional cancer cell migration by aligning fibronectin. J Cell Biol 216, 3799–3816.

Eyckmans J, Chen CS (2017). 3D culture models of tissues under tension. J Cell Sci 130, 63–70.

Frantz C, Stewart KM, Weaver VM (2010). The extracellular matrix at a glance. J Cell Sci 123, 4195–4200.

Galloway MT, Lalley AL, Shearn JT (2013). The role of mechanical loading in tendon development, maintenance, injury, and repair. J Bone Joint Surg Am 95, 1620–1628.

Greiner AM, Chen H, Spatz JP, Kemkemer R (2013). Cyclic tensile strain controls cell shape and directs actin stress fiber formation and focal adhesion alignment in spreading cells. PLoS One 8, e77328.

Hanley CJ, Noble F, Ward M, Bullock M, Drifka C, Mellone M, Manousopoulou A, Johnston HE, Hayden A, Thirdborough S, *et al.* (2016). A subset of myofibroblastic cancer-associated fibroblasts regulate collagen fiber elongation, which is prognostic in multiple cancers. Oncotarget 7, 6159–6174.

Harris GM, Raitman I, Schwarzbauer JE (2018). Cell-derived decellularized extracellular matrices. Methods Cell Biol 143, 97–114.

Hassell JR, Birk DE (2010). The molecular basis of corneal transparency. Exp Eye Res 91, 326–335.

Hayakawa K, Sato N, Obinata T (2001). Dynamic reorientation of cultured cells and stress fibers under mechanical stress from periodic stretching. Exp Cell Res 268, 104–114.
Heidari M, Mandato CA, Lehoux S (2015). Vascular smooth muscle cell phenotypic modulation and the extracellular matrix. Artery Research 9.
Huang C, Fu X, Liu J, Qi Y, Li S, Wang H (2012). The involvement of integrin beta1 signaling in the migration and myofibroblastic differentiation of skin fibroblasts on anisotropic collagen-containing nanofibers. Biomaterials 33, 1791–1800.
Karamichos D, Hutcheon AE, Zieske JD (2011). Transforming growth factor-beta3 regulates assembly of a non-fibrotic matrix in a 3D corneal model. J Tissue Eng Regen Med 5, e228–e238.
Kim HN, Jiao A, Hwang NS, Kim MS, Kang DH, Kim DH, Suh KY (2013). Nanotopography-guided tissue engineering and regenerative medicine. Adv Drug Deliv Rev 65, 536–558.
Kinsey R, Williamson MR, Chaudhry S, Mellody KT, McGovern A, Takahashi S, Shuttleworth CA, Kielty CM (2008). Fibrillin-1 microfibril deposition is dependent on fibronectin assembly. J Cell Sci 121, 2696–2704.
Kjaer M (2004). Role of extracellular matrix in adaptation of tendon and skeletal muscle to mechanical loading. Physiol Rev 84, 649–698.
Kloeker S, Major MB, Calderwood DA, Ginsberg MH, Jones DA, Beckerle MC (2004). The Kindler syndrome protein is regulated by transforming growth factor-beta and involved in integrin-mediated adhesion. J Biol Chem 279, 6824–6833.
Lanfer B, Freudenberg U, Zimmermann R, Stamov D, Korber V, Werner C (2008). Aligned fibrillar collagen matrices obtained by shear flow deposition. Biomaterials 29, 3888–3895.
Li Y, Huang G, Zhang X, Wang L, Du Y, Lu TJ, Xu F (2014). Engineering cell alignment in vitro. Biotechnol Adv 32, 347–365.
Liu CF, Aschbacher-Smith L, Barthelery NJ, Dyment N, Butler D, Wylie C (2012). Spatial and temporal expression of molecular markers and cell signals during normal development of the mouse patellar tendon. Tissue Eng Part A 18, 598–608.
Livne A, Bouchbinder E, Geiger B (2014). Cell reorientation under cyclic stretching. Nat Commun 5, 3938.
Livne A, Geiger B (2016). The inner workings of stress fibers—from contractile machinery to focal adhesions and back. J Cell Sci 129, 1293–1304.
Malandrino A, Trepat X, Kamm RD, Mak M (2019). Dynamic filopodial forces induce accumulation, damage, and plastic remodeling of 3D extracellular matrices. PLoS Comput Biol 15, e1006684.
Marthandan S, Priebe S, Baumgart M, Groth M, Cellerino A, Guthke R, Hemmerich P, Diekmann S (2015). Similarities in gene expression profiles during in vitro aging of primary human embryonic lung and foreskin fibroblasts. Biomed Res Int 2015, 731938.
McKee TJ, Perlman G, Morris M, Komarova SV (2019). Extracellular matrix composition of connective tissues: a systematic review and meta-analysis. Sci Rep 9, 10542.
McKeown-Longo PJ, Mosher DF (1985). Interaction of the 70,000-mol-wt amino-terminal fragment of fibronectin with the matrix-assembly receptor of fibroblasts. J Cell Biol 100, 364–374.
Meek KM, Knupp C (2015). Corneal structure and transparency. Prog Retin Eye Res 49, 1–16.
Midwood KS, Schwarzbauer JE (2002). Tenascin-C modulates matrix contraction via focal adhesion kinase- and Rho-mediated signaling pathways. Mol Biol Cell 13, 3601–3613.
Miller CG, Pozzi A, Zent R, Schwarzbauer JE (2014). Effects of high glucose on integrin activity and fibronectin matrix assembly by mesangial cells. Mol Biol Cell 25, 2342–2350.
Pankov R, Cukierman E, Katz BZ, Matsumoto K, Lin DC, Lin S, Hahn C, Yamada KM (2000). Integrin dynamics and matrix assembly: tensin-dependent translocation of alpha(5)beta(1) integrins promotes early fibronectin fibrillogenesis. J Cell Biol 148, 1075–1090.
Paszek MJ, Weaver VM (2004). The tension mounts: mechanics meets morphogenesis and malignancy. J Mammary Gland Biol Neoplasia 9, 325–342.
Piotrowski-Daspit AS, Nerger BA, Wolf AE, Sundaresan S, Nelson CM (2017). Dynamics of tissue-induced alignment of fibrous extracellular matrix. Biophys J 113, 702–713.
Provenzano PP, Eliceiri KW, Campbell JM, Inman DR, White JG, Keely PJ. (2006). Collagen reorganization at the tumor-stromal interface facilitates local invasion. BMC Med 4, 38.
Provenzano PP, Inman DR, Eliceiri KW, Knittel JG, Yan L, Rueden CT, White JG, Keely PJ (2008). Collagen density promotes mammary tumor initiation and progression. BMC Med 6, 11.
Pryce BA, Watson SS, Murchison ND, Staverosky JA, Dunker N, Schweitzer R (2009). Recruitment and maintenance of tendon progenitors by TGFbeta signaling are essential for tendon formation. Development 136, 1351–1361.
Puspoki Z, Storath M, Sage D, Unser M (2016). Transforms and operators for directional bioimage analysis: a survey. Adv Anat Embryol Cell Biol 219, 69–93.
Rezakhaniha R, Agianniotis A, Schrauwen JT, Griffa A, Sage D, Bouten CV, van de Vosse FN, Unser M, Stergiopulos N (2012). Experimental investigation of collagen waviness and orientation in the arterial adventitia using confocal laser scanning microscopy. Biomech Model Mechanobiol 11, 461–473.
Romereim SM, Conoan NH, Chen B, Dudley AT (2014). A dynamic cell adhesion surface regulates tissue architecture in growth plate cartilage. Development 141, 2085–2095.
Sabatier L, Chen D, Fagotto-Kaufmann C, Hubmacher D, McKee MD, Annis DS, Mosher DF, Reinhardt DP (2009). Fibrillin assembly requires fibronectin. Mol Biol Cell 20, 846–858.
Sarkar S, Dadhania M, Rourke P, Desai TA, Wong JY (2005). Vascular tissue engineering: microtextured scaffold templates to control organization of vascular smooth muscle cells and extracellular matrix. Acta Biomater 1, 93–100.
Schwarzbauer JE, DeSimone DW (2011). Fibronectins, their fibrillogenesis, and in vivo functions. Cold Spring Harb Perspect Biol 3.
Singh P, Carraher C, Schwarzbauer JE (2010). Assembly of fibronectin extracellular matrix. Annu Rev Cell Dev Biol 26, 397–419.
Singh S, Bandini SB, Donnelly PE, Schwartz J, Schwarzbauer JE (2014). A cell-assembled, spatially aligned extracellular matrix to promote directed tissue development. J Mater Chem B 2, 1449–1453.
Sivakumar P, Czirok A, Rongish BJ, Divakara VP, Wang YP, Dallas SL (2006). New insights into extracellular matrix assembly and reorganization from dynamic imaging of extracellular matrix proteins in living osteoblasts. J Cell Sci 119, 1350–1360.
Sottile J, Hocking DC (2002). Fibronectin polymerization regulates the composition and stability of extracellular matrix fibrils and cell-matrix adhesions. Mol Biol Cell 13, 3546–3559.
Sottile J, Shi F, Rublyevska I, Chiang HY, Lust J, Chandler J (2007). Fibronectin-dependent collagen I deposition modulates the cell response to fibronectin. Am J Physiol Cell Physiol 293, C1934–C1946.
Stanchi F, Grashoff C, Nguemeni Yonga CF, Grall D, Fassler R, Van Obberghen-Schilling E (2009). Molecular dissection of the ILK-PINCH-parvin triad reveals a fundamental role for the ILK kinase domain in the late stages of focal-adhesion maturation. J Cell Sci 122, 1800–1811.
Sun Z, Costell M, Fassler R (2019). Integrin activation by talin, kindlin and mechanical forces. Nat Cell Biol 21, 25–31.
Theodosiou M, Widmaier M, Bottcher RT, Rognoni E, Veelders M, Bharadwaj M, Lambacher A, Austen K, Muller DJ, Zent R, Fassler R (2016). Kindlin-2 cooperates with talin to activate integrins and induces cell spreading by directly binding paxillin. Elife 5, e10130.
Thery M (2010). Micropatterning as a tool to decipher cell morphogenesis and functions. J Cell Sci 123, 4201–4213.
Thery M, Pepin A, Dressaire E, Chen Y, Bornens M (2006). Cell distribution of stress fibres in response to the geometry of the adhesive environment. Cell Motil Cytoskeleton 63, 341–355.
Tomasek JJ, Gabbiani G, Hinz B, Chaponnier C, Brown RA (2002). Myofibroblasts and mechano-regulation of connective tissue remodelling. Nat Rev Mol Cell Biol 3, 349–363.
Velling T, Risteli J, Wennerberg K, Mosher DF, Johansson S (2002). Polymerization of type I and III collagens is dependent on fibronectin and enhanced by integrins alpha 11beta 1 and alpha 2beta 1. J Biol Chem 277, 37377–37381.
Wang JH, Jia F, Gilbert TW, Woo SL (2003). Cell orientation determines the alignment of cell-produced collagenous matrix. J Biomech 36, 97–102.
Wang JH, Yang G, Li Z, Shen W (2004). Fibroblast responses to cyclic mechanical stretching depend on cell orientation to the stretching direction. J Biomech 37, 573–576.
Wilson CL, Schwarzbauer JE (1992). The alternatively spliced V region contributes to the differential incorporation of plasma and cellular fibronectins into fibrin clots. J Cell Biol 119, 923–933.
Zamir E, Katz M, Posen Y, Erez N, Yamada KM, Katz BZ, Lin S, Lin DC, Bershadsky A, Kam Z, Geiger B (2000). Dynamics and segregation of cell-matrix adhesions in cultured fibroblasts. Nat Cell Biol 2, 191–196.
Zhang Q, Checovich WJ, Peters DM, Albrecht RM, Mosher DF (1994). Modulation of cell surface fibronectin assembly sites by lysophosphatidic acid. J Cell Biol 127, 1447–1459.
Zhong C, Chrzanowska-Wodnicka M, Brown J, Shaub A, Belkin AM, Burridge K (1998). Rho-mediated contractility exposes a cryptic site in fibronectin and induces fibronectin matrix assembly. J Cell Biol 141, 539–551.